Journal of Hazardous Materials 460 (2023) 132363

Contents lists available at ScienceDirect

Journal of Hazardous Materials

journal homepage: www.elsevier.com/locate/jhazmat

Research Paper

Insight into the selection of oxidant in persulfate activation system: The effect of the target pollutant properties

Xuerong Zhou [a], Eydhah Almatrafi [b], Shiyu Liu [a], Huchuan Yan [a], Dengsheng Ma [a], Shixian Qian [a], Lei Qin [a], Huan Yi [a], Yukui Fu [a], Ling Li [a], Mingming Zhang [a], Fuhang Xu [a], Hanxi Li [a], Chengyun Zhou [a,b], Ming Yan [a,b], Guangming Zeng [a,b,*], Cui Lai [a,**]

[a] College of Environmental Science and Engineering, Hunan University and Key Laboratory of Environmental Biology and Pollution Control, Hunan University, Ministry of Education, Changsha 410082, PR China

[b] Center of Research Excellence in Renewable Energy and Power Systems, Center of Excellence in Desalination Technology, Department of Mechanical Engineering, Faculty of Engineering-Rabigh, King Abdulaziz University, Jeddah 21589, Saudi Arabia

HIGHLIGHTS

- The properties of target pollutant would influence the superior persulfate species.
- E_{HOMO} and VIP of pollutant can be applied to judge the superior persulfate species.
- Co-existing cations of PDS showed little effect on heterogeneous catalysis.
- The superior peroxydisulfate species were not affected by the target pollutants.

GRAPHICAL ABSTRACT

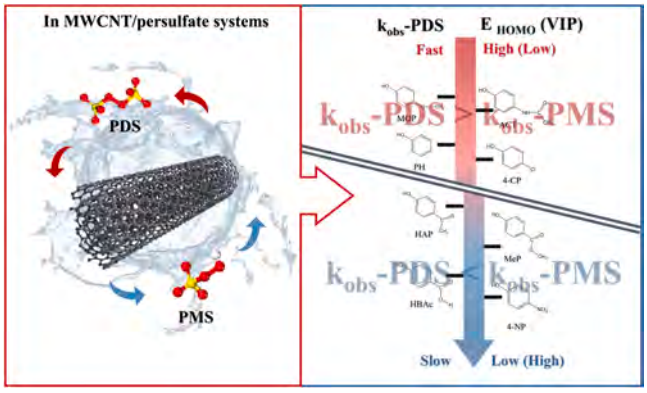

ARTICLE INFO

Editor: Baiyang Chen

Keywords:
Multiwalled carbon nanotube
Superior persulfate species
Peroxymonosulfate
Peroxydisulfate
Phenolic compounds

ABSTRACT

As a rising branch of advanced oxidation processes, persulfate activation has attracted growing attention. Unlike catalysts that have been widely studied, the selection of persulfate is previously overlooked. In this study, the affecting factors of persulfates were studied. The effect of target pollutant properties on superior persulfate species (the species with a higher degradation efficiency) was investigated by multiwalled carbon nanotube (MWCNT)/persulfate catalytic systems. Innovatively, the E_{HOMO} (or vertical ionization potential (VIP)) value of the target pollutant was proposed to be an index to judge the superior persulfate species, and the threshold is VIP= 6.397–6.674 eV, E_{HOMO}= −8.035~− 7.810 eV, respectively. To be specific, when the VIP of phenolic compounds is higher (or E_{HOMO} of phenolic compounds is lower) than the threshold, the catalytic performance of peroxymonosulfate would be higher than that of peroxydisulfate. Moreover, the effects of coexisting cations on

* Corresponding author at: College of Environmental Science and Engineering, Hunan University and Key Laboratory of Environmental Biology and Pollution Control, Hunan University, Ministry of Education, Changsha 410082, PR China.
** Corresponding author.
E-mail addresses: zgming@hnu.edu.cn (G. Zeng), laicui@hnu.edu.cn (C. Lai).

https://doi.org/10.1016/j.jhazmat.2023.132363
Received 31 May 2023; Received in revised form 7 August 2023; Accepted 20 August 2023
Available online 22 August 2023

peroxydisulfate superior species were further investigated. It was illustrated that the hydrated cation radius of coexisting cations would influence the pollutant degradation efficiency under some circumstances. This study provides a new approach to improve the cost of persulfate activation systems and promotes the underlying downstream application of persulfate activation systems.

1. Introduction

Advanced oxidation processes (AOPs) are recognized as effective chemical technologies, which mainly treat with refractory organic compounds by strong reactive active species (such as $SO_4^{\bullet-}$, $^{\bullet}OH$, $O_2^{\bullet-}$, and $^1O_2$) [1]. As a high-efficiency and low-cost branch of AOPs (including Fenton oxidation [2–4], electrocatalysis [5], photocatalysis [6–9], ozonation [10], etc.), the persulfate activation technique has attracted wide concern in the past decade [11–13]. Different from other AOPs (such as Fenton oxidation system and ozonation systems), there are many choices of oxidants in the persulfate activation system. In terms of coexisting cations, sodium peroxydisulfate (PDS-Na), potassium peroxydisulfate (PDS) and ammonium peroxydisulfate (PDS-NH_4) are all available oxidants. Besides, depending on the active anion, PDS and peroxymonosulfate (PMS) are also common options. Spontaneously, the selection of superior oxidants becomes a unique subject in persulfate activation.

As mentioned above, the distinction between PDS and PMS is the difference in the persulfate anion ($S_2O_8^{2-}$ or HSO_5^-). Generally, the bond energies of O-O bonds in persulfate anions are extensively used as the basis for determining the superior persulfate species. To be specific, the O-O bond energy of PDS is 92 kJ·mol^{-1}, which is lower than that of PMS (377 kJ·mol^{-1}) [14,15]. It is indicated PDS is more easily decomposed, supporting that the PDS-induced system has better pollutant degradation performance. However, conflicting conclusion was conducted by other studies. It was explained that the symmetrical structure hampered the decomposition of PDS, which made the catalytic performance of the PDS-induced system was likely to lower than that of PMS [16,17]. In short, the catalytic performance of the PDS-induced system and PMS-induced system cannot be generalized to date. There is no doubt that the selection of suitable oxidant is an effective means of reducing costs, which can ultimately promote the downstream application of persulfate activation systems. Thus, it is of great significance to dig out the underlying mechanisms and influencing factors of superior persulfate species.

Among the factors influencing persulfate activation systems, the role of target pollutant is often neglected. It has been reported that the bromophenols degradation ability of PDS was stronger than PMS in nanotube-induced systems [18]. When phenol was selected as the target pollutant, the catalytic performance of the PMS-induced system was observably higher than that of PDS [16]. Given this, it is reasonable to speculate that the target pollutant might influence the superior persulfate species. Recently, the properties of the target pollutant have been verified to affect its degradation efficiency and mechanism in the persulfate activation system. To be specific, the pollutants with high highest occupied molecular orbital (E_{HOMO}) and low energy gap of E_{HOMO} and E_{LUMO} (ΔE) were preferred to be attacked in persulfate activation systems [19]. Similarly, the half-wave potential, an electrochemical index to appraise the redox capacity of compounds, has been also reported as closely associated with the degradation efficiency [20]. Furthermore, a strong correlation between hydrophobicity and pollutant degradation rate has been reported lately [21]. Based on these, the target pollutant may be considered as one of the factors affecting the superior persulfate species.

In the persulfate activation systems, the application of highly efficient metal-based catalysts is accompanied by the leaching of heavy metal, which puts pressure on the secondary sludge purification and ecosystem [22,23]. Consequently, carbonaceous materials (such as graphite, graphene, fullerene, and carbon nanotubes) were repeatedly introduced in persulfate activation [24]. At the state of the art, numerous studies were launched to improve the activation efficiency of carbonaceous materials. In general, elements doping, chemical modification, and metal loading are common approaches to enhance the activation capacity of carbonaceous materials [25]. However, these modification methods can complicate the degradation mechanism of persulfate activation systems. Given this, multiwalled carbon nanotube (MWCNT), one of the benchmark carbonaceous materials, was introduced in the persulfate activation system to probe into the effect of the characteristics of pollutants on the superior persulfate species [26–28].

In this study, the MWCNT/persulfate system was applied as the model system. Besides, as a widespread class of organic compounds with ecotoxicity, phenolic compounds were used as target pollutants [29–31]. Firstly, according to previous studies, the superior persulfate species would change when the target pollutant was changed from acetaminophen (ACT) to methylparaben (MeP) [17,24]. Thus, ACT and MeP were chosen as the typical target pollutants to explore mechanistic changes brought about by target pollutants. Approaches such as active species capture experiments were applied to estimate the distinction in degradation mechanism in the MWCNT/persulfate systems. Subsequently, in order to further probe the effect of the target pollutant on the superior species of persulfates, 8 phenolic compounds with similar molecular structures were introduced. Density functional theory calculations (DFT calculations, such as E_{HOMO}, E_{LUMO}, ΔE, etc.) were employed to theoretically delve into the specific effect of pollutant properties on superior persulfate species. Finally considering that depending on the coexisting cations, peroxydisulfates (PDSs) can be divided into PDS, sodium PDS-Na, and PDS-NH_4. The effects of co-existing cations on pollutant degradation and whether the superior PDSs species are influenced by the pollutant were explored.

2. Materials and methods

2.1. Chemical reagent

The details of involved chemical reagents were listed in Text S1.

2.2. Experimental process

All batches were operated at room temperate and taken in 100 mL beakers. Firstly, 0.10 g/L MWCNT was stirred in 20 mg/L (or 2 mM) target pollutant solution (ACT, MeP, and other involved compounds) to reach the adsorption/desorption equilibrium. After stirring for 1 h, the catalytic process was triggered with 4 mM persulfate (PMS, PDS, PDS-Na, or PDS-NH_4). Samples were collected at the predetermined time. 0.22 μm nylon filter was applied to remove the particles, and 0.50 M $Na_2S_2O_3$ was used to terminate the reaction. The concentration of phenolic compounds was measured by high performance liquid chromatography (HPLC, Agilent 1200), which was armed with a C18 column (5 μm, 4.60 mm × 250 mm). Methanol, acetonitrile, 0.1% acetic acid, and 0.1% formic acid were applied as the mobile phase (the specific analysis methods were listed in Table S1). The degradation rate was evaluated by Eq. 1 (pseudo-first-order kinetics model) [32,33].

$$\ln\left(\frac{C_t}{C_0}\right) = -k_{obs}t \quad (1)$$

Where t (min) is the sampling time, C_t (mg/L) represents the phenolic compound concentration of each sample, and C_0 (mg/L) is the initial concentration of phenolic compounds. k_{obs} is the pseudo-first-order rate

constant that is used to quantitatively evaluate the performance of different persulfate activation systems.

In the active species capture experiment, ethanol (EtOH), tert-butyl alcohol (TBA), *p*-benzoquinone (BQ), and furfuryl alcohol (FFA) were applied to selectively capture $SO_4^{\bullet-}$, $^{\bullet}OH$, $O_2^{\bullet-}$, and $^1O_2$ (The trapping agent was added before the adsorption process). Additionally, 1,3-diphenylisobenzofuran (DPBF, 0.05 mM) could react with $^1O_2$ in a molar ratio of 1:1, and the consumption amount of DPBF could be detected by an ultraviolet spectrophotometer. Consequently, it was employed to quantitate the amount of $^1O_2$ in persulfate activation systems.

2.3. Characterization and analytical methods

X-ray photoelectron spectroscopy (XPS, Thermo Scientific K-Alpha), automatic specific surface and porosity analyzer (Micromeritics ASAP 2460), and Raman spectra (Renishaw invia reflex, LabRam HR Evolution) were involved to get the information of MWCNT. The concentration of DPBF was detected by UV spectrophotometer (Shimadzu UV2700). Liner sweep voltammetry (LSV) and open circuit potential curves were measured in 0.1 M Na_2SO_4 and taken on CHI760E electrochemical workstation (the calomel electrode was the reference electrode, and the platinum electrode was the counter electrode). The electron spin resonance analysis (ESR, JES-FA200) was employed to identify the active species. 5,5-dimethyl-1-pyrroline N-oxide (DMPO) was used as the trapping agent for $^{\bullet}OH$, $SO_4^{\bullet-}$, and $O_2^{\bullet-}$, and 2,2,6,6-tetramethylpiperidine (TEMP) could preferentially capture $^1O_2$ in aqueous media. Xlog P is a common theoretical parameter to appraise the hydrophobicity of organic compounds. A higher value of Xlog P indicated stronger hydrophobicity. The value of Xlog P was acquired from websites: https://pubchem.ncbi.nlm.nih.gov/.

2.4. DFT calculation details

To dig into the structural differences of organic compounds, DFT calculations were launched using Gaussian 16 package [34]. Geometry optimizations were conducted at the B3LYP/6–311 G(d,p) level of theory with Grimme's empirical dispersion correction [35–37]. Frequency analysis was involved to get the thermal corrections and confirm the stationary points as minima. The energies of HOMO (E_{HOMO}) and LUMO (E_{LUMO}) of the optimized structures were calculated using the M06–2X functional applied with the def2-TZVP basis [38], which was introduced for single-point energy calculations. Solvation effects were involved in all calculations. In this study, water was appointed as the solvent which was simulated by the integral equation formalism polarizable continuum model (IEF-PCM) [39]. The vertical ionization potential (VIP) was obtained by Eq. S1.

$$VIP=E_{(N-1)}-E_{(N)} \quad (S1)$$

Where $E_{(N-1)}$ represents the energy of the optimized energy of the charged state pollutant in the most stable geometry, and the $E_{(N)}$ is ascribed to the optimized energy of the pollutant in the most stable geometry.

The detail of Fukui function calculation was provided in Text S2 [40,41].

2. Results and discussion

3.1. Catalyst Structure and Properties

Understanding the basic structure information of the catalyst can favor the further analysis of its catalytic performance. In this study, XPS, Raman spectra, and BET were taken to probe the properties of involved MWCNT. Specifically, N_2 adsorption and desorption analysis manifested that the specific surface area and pore volume of MWCNT was 97.43 m^2/g and 0.50 cm^3 /g, respectively (Fig. S1a). When it comes to the defect and graphitization degree, the Raman spectra exhibited obvious MWCNT signatures [42]. As shown in Fig. S1b, the band around 1580 cm^{-1} ascribed to the in-plane vibration of the C–C bond (G band), which represented the degree of graphitization. The band around 1350 cm^{-1} was assigned to a disorder breaking in MWCNT structure (D band), while the band at 2680 cm^{-1} corresponded to two-phonon scattering in MWCNT (2D band) [29,42,43]. Furthermore, the intensity ratio of D band and G band (I_D/I_G) universally reflected the disorder degree of carbonaceous materials, and the value of the involved MWCNT was 0.6021. XPS spectra was applied to investigate the surface element composition. As shown in Fig. S1c, a hint of O atom (1.6 at%) was detected, which verified the existence of oxygen-containing groups on involved MWCNT. To ascertain the proportion of different oxygen-containing groups, high resolution scan of C 1 s was taken (Fig. S1d). C 1 s peak was deconvoluted into four peaks. The peak located at 284.80, 285.95, 288.5, and 291.27 eV were assigned to the vibration of C-C, C-O, C═O, and π-π * shake-up, respectively [44]. Among them, π-π * shake-up represented satellite structure results from the extended delocalized electrons (such as aromatic rings) in MWCNT [45]. The peaks of C-O and C═O could roughly reflect the distribution of oxygen-containing groups on MWCNT. Concretely, C-O and C═O accounted for 18.78% and 4.41%, respectively.

3.2. Persulfate activation with MWCNT

As mentioned above, carbonaceous materials have been repeatedly applied to activate persulfate. However, the superior persulfate species (PDS or PMS) differed in different persulfate activation systems. It supported that the superior persulfate species was not only influenced by the nature of persulfate itself. Consequently, it is necessary to investigate the factors affecting the superior persulfate species and the underlying influencing mechanism.

In preliminary experiments, the significant role of target pollutants on superior persulfate species (PDS and PMS) was noted [17,24]. Using MWCNT/persulfate systems as the model system, the catalytic experiments showed that the superior persulfate species would vary with the change of targeted pollutants. Concretely, the ACT degradation rate in MWCNT/PMS system was 0.0423 min^{-1}, and it could reach 0.2778 min^{-1} in the MWCNT/PDS system. Whereas when MeP was selected as the target pollutant, the catalytic performance of the MWCNT/PMS (0.0077 min^{-1} versus 0.0044 min^{-1} of the MWCNT/PDS system) system was better (Fig. 1). This phenomenon manifested that the target pollutant would affect the superior persulfate species.

To distinguish structural differences between PDS and PMS, the bond

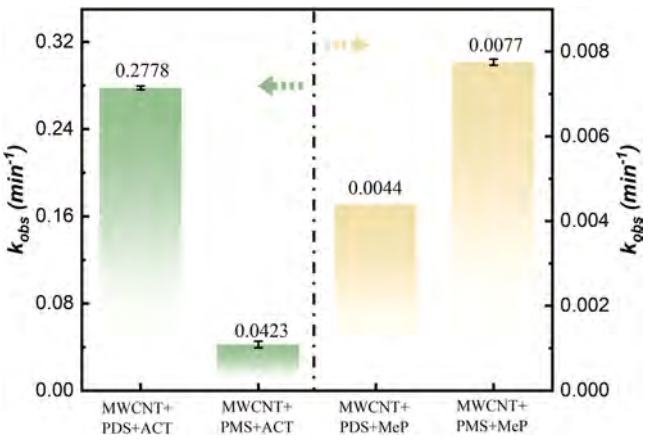

Fig. 1. Catalytic performance of MWCNT/PDS and MWCNT/PMS systems. [Experimental conditions]: [MWCNT]= 0.10 g/L, [Persulfate]= 1 g/L, [Pollutant]= 20 mg/L.

length and bond energy of the important reactive structure (O-O bonds) were estimated using theoretical calculations. Generally, bond with short length and high energy is hard to be broken. In persulfate activation systems, the catalytic activity of peroxide generally expresses by the bond energy and bond length of O-O bond. DFT calculations were applied to acquire the theoretical bond length and energy of PDS and PMS. As shown in Table S2, the O-O bond in PMS (1.443 Å, 177.89 kJ/mol) is stronger than that of PDS (1.451 Å, 107.68 kJ/mol). It was supported that the PDS possessed a higher catalytic activity than PMS. This conclusion was further verified by the result of the thermal activation system. Theoretically, the thermal activation process can achieve energy input without introducing other substances. Thus, the thermal activation process was applied to evaluate the strength and thermal stability of O-O bond in persulfate (PDS and PMS). According to Table S3, PDS showed a higher degradation ability to both ACT and MeP. The influence of pollutants on superior persulfate species was not obvious in thermal activation systems. However, the superior persulfate species varied with the target pollutant has been observed in MWCNT/persulfate systems. It is reasonable to deduce that the introduction of MWCNT brought about a brand-new degradation mechanism independent of the breaking of O-O bond.

To probe into the difference in degradation mechanism between MWCNT/PDS and MWCNT/PMS systems, active species capture experiments and ESR spectra were taken. The results of ESR spectra illustrated that all four common active species existed in both MWCNT/PDS and MWCNT/PMS systems (Fig. S2). The contribution of different active species was further verified by active species capture experiments. EtOH, TBA, BQ, and FFA were used to selectively capture $SO_4^{\bullet-}$, $^{\bullet}OH$, $O_2^{\bullet-}$, and $^1O_2$ in persulfate activation systems. As shown in Fig. 2 and Fig. S3, broadly speaking, the inhibitory effects of radical trapping agents were more pronounced in MWCNT/PMS system than that in MWCNT/PDS system. Moreover, since BA cannot be degraded by electron transfer pathway and other active species, it was chosen as a probe for radicals [46,47]. As shown in Fig. S4, the degradation efficiency of BA in the PMS-induced system (0.00215 min^{-1}) was faster than that in the PDS-induced system (0.0007 min^{-1}). It was indicated that the contribution of radicals is greater in the MWCNT/PMS system compared to the MWCNT/PDS system.

Thereinto, BQ exhibited the strongest inhibitory effect as a trapping agent of $O_2^{\bullet-}$ when ACT was the target pollutant. However, it has been proved that $O_2^{\bullet-}$ could not directly react with ACT [48]. The strong inhibitory effect of BQ might be associated with the following two reasons. On the one hand, the second-order rate of BQ with $SO_4^{\bullet-}$ and $^{\bullet}OH$ were relatively high (Table S4). It was implied that the inhibitory effect of BQ was not only brought by quenching $O_2^{\bullet-}$. On the other hand, $O_2^{\bullet-}$ is liable to transfer to $^1O_2$ at acid condition (Eq. 2, the reaction rate is $2.4 \times 10^{12-pH}$ M^{-1} s^{-1}) [49]. Thus, the addition of BQ would impair the yield of $^1O_2$, whose second-order rate constants with ACT could reach 3.35×10^6 $M^{-1}s^{-1}$ (Table S4). Ultimately, the apparent degradation efficiency was significantly inhibited by BQ.

$$2H^+ + \quad 2O_2^{\bullet-} \rightarrow {}^1 \quad O_2 + \quad H_2O_2 \tag{2}$$

Furthermore, the contribution of $^1O_2$ was evaluated by FFA. The second-order rate constant of FFA (1.2×10^8 M^{-1} s^{-1}) with $^1O_2$ was

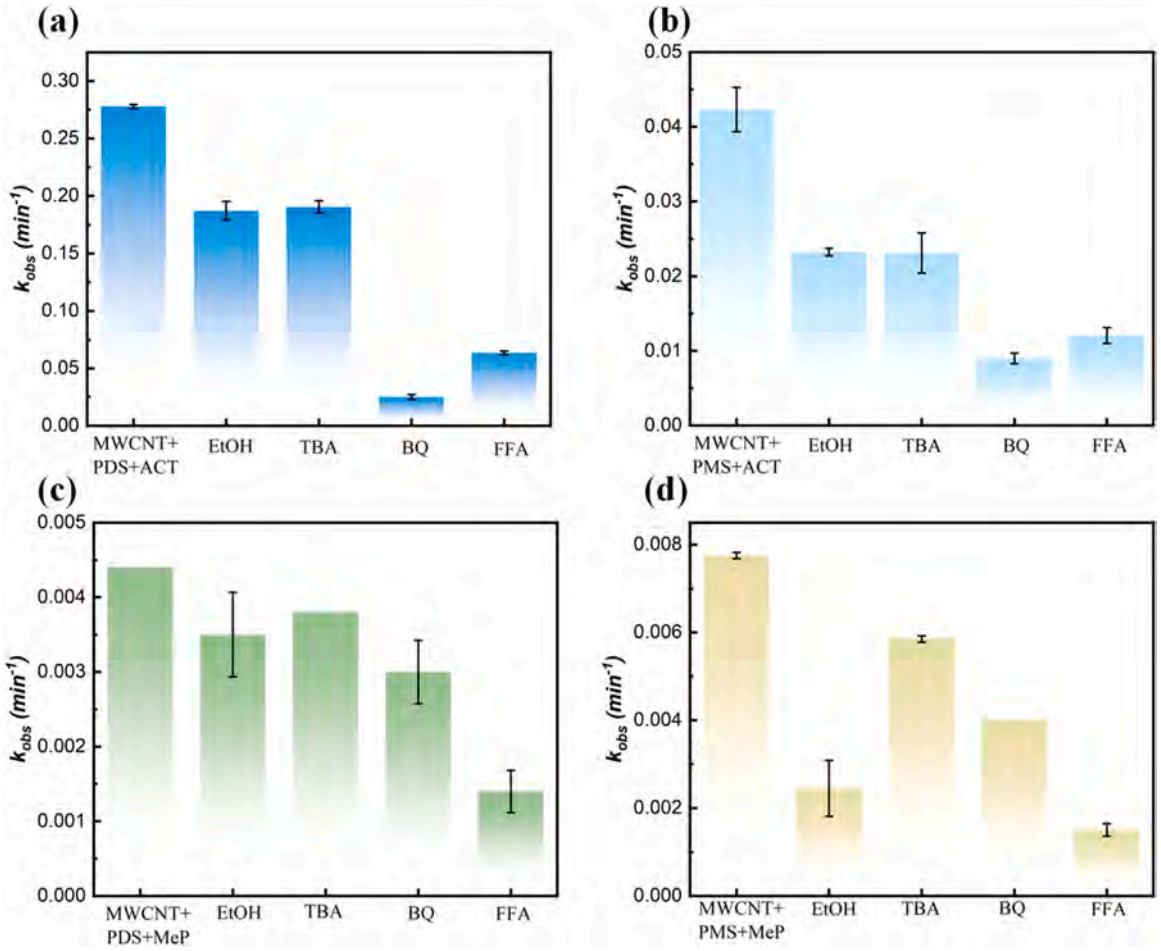

Fig. 2. Active species capture experiment and corresponding pseudo-first-order rate constants of (a) MWCNT/PDS/ACT system, (b) MWCNT/PMS/ACT system, (c) MWCNT/PDS/MeP system, and (d) MWCNT/PMS/MeP system. [Experimental conditions]: [MWCNT]= 0.10 g/L, [Persulfate]= 4 mM, [Pollutant]= 20 mg/L, [EtOH] = 40 mM, [TBA] = 40 mM, [BQ] = 1 mM, [FFA] = 40 mM.

considerably higher than that of phenolic compounds (2–3 $\times 10^6$ M^{-1} s^{-1}) [50]. The active species capture experiments illustrated that FFA significantly inhibited the degradation process. Nevertheless, it could not support the primary role of $^1O_2$ in the persulfate activation system, because FFA also showed relatively high reactivity with other active species (such as $SO_4^{\bullet-}$ and $^{\bullet}OH$) and persulfate [51]. Thus, DPBF (0.05 mM) was introduced for the quantification of $^1O_2$ in the persulfate activation systems [13]. As shown in Fig. S5a-b, different from PDS, PMS could produce $^1O_2$ by self-decomposition [52]. Furthermore, the $^1O_2$ generation process was distinctly facilitated by MWCNT in the persulfate activation system (Fig. 5c-d). 99.1% DPBF was consumed within 6 min in MWCNT/PMS system, and the MWCNT/PDS system only degrade 15.1% DPBF within 60 min. Intuitively (Fig. S6), there was almost no change in the MWCNT/PDS system after a 60 min decolorization reaction, while the DPBF in the MWCNT/PMS system almost completely faded. Besides, the decolorization process of DPBF could help quantify $^1O_2$ for DPBF reacts with $^1O_2$ in a molar ratio of 1:1 [53]. That is, more than 4.95 mmol•g^{-1}•L of $^1O_2$ was produced in MWCNT/PMS system, while 0.76 mmol•g^{-1}•L $^1O_2$ was generated in MWCNT/PDS system. However, the extreme difference in the amount of $^1O_2$ did not result in a distinct difference in the pollutant degradation efficiency. Additionally, the MWCNT/PMS system, which produced more $^1O_2$ was less efficient at degrading ACT than the MWCNT/PDS system. Considering the low second-order rate constants of $^1O_2$ with both ACT and MeP (~10^6 M^{-1} s^{-1}) [50,54], it is reasonable to assume that $^1O_2$ did not play a central role in MWCNT/persulfate systems.

The experimental results indicated that the effect of active species on pollutant degradation was more pronounced in the MWCNT/PMS system than in the MWCNT/PDS system. However, from another perspective, the relatively low degradation efficiency of radical probe (BA) in both PDS-induced and PMS-induced systems, and the variation in the amount of $^1O_2$ exhibited little effect on the pollutant degradation efficiency. These supported that there might be another mechanism that dominated the degradation process of MWCNT/PMS and MWCNT/PDS systems.

Aside from active species, the persulfate activation system can degrade organic pollutants by electron transfer pathway. As is well known, the electron transfer pathway relies on the formation of ternary construction (catalyst-persulfate-pollutant), which can transfer electrons from pollutants to persulfate without producing active species. LSV is an effective method for confirming the existence of the electron transfer pathway [55]. The results illustrated the current reached its maximum that only when pollutants, MWCNT, and persulfates were present at the same time (Fig. S7). It was supported that ACT and MeP could be degraded by electron transfer pathways in both MWCNT/PMS and MWCNT/PDS systems. Open circuit potential curve was another approach to investigate the electron transfer pathway in the persulfate activation system. As shown in Fig. 3a-b, the curves of open circuit potential experienced a visible decline after the addition of pollutants. This was strong evidence that the electron transfer pathway occurred.

Ulteriorly, the variation of LSV and open circuit potential are applied to assess the strength of the electron transfer pathway [56,57]. In terms of LSV (Fig. 3c-d), in the MWCNT/PMS system, the current at 1.50 V was 3.889 $\times$ 10^{-4} and 4.766 $\times$ 10^{-4} mA for target pollutants ACT and MeP,

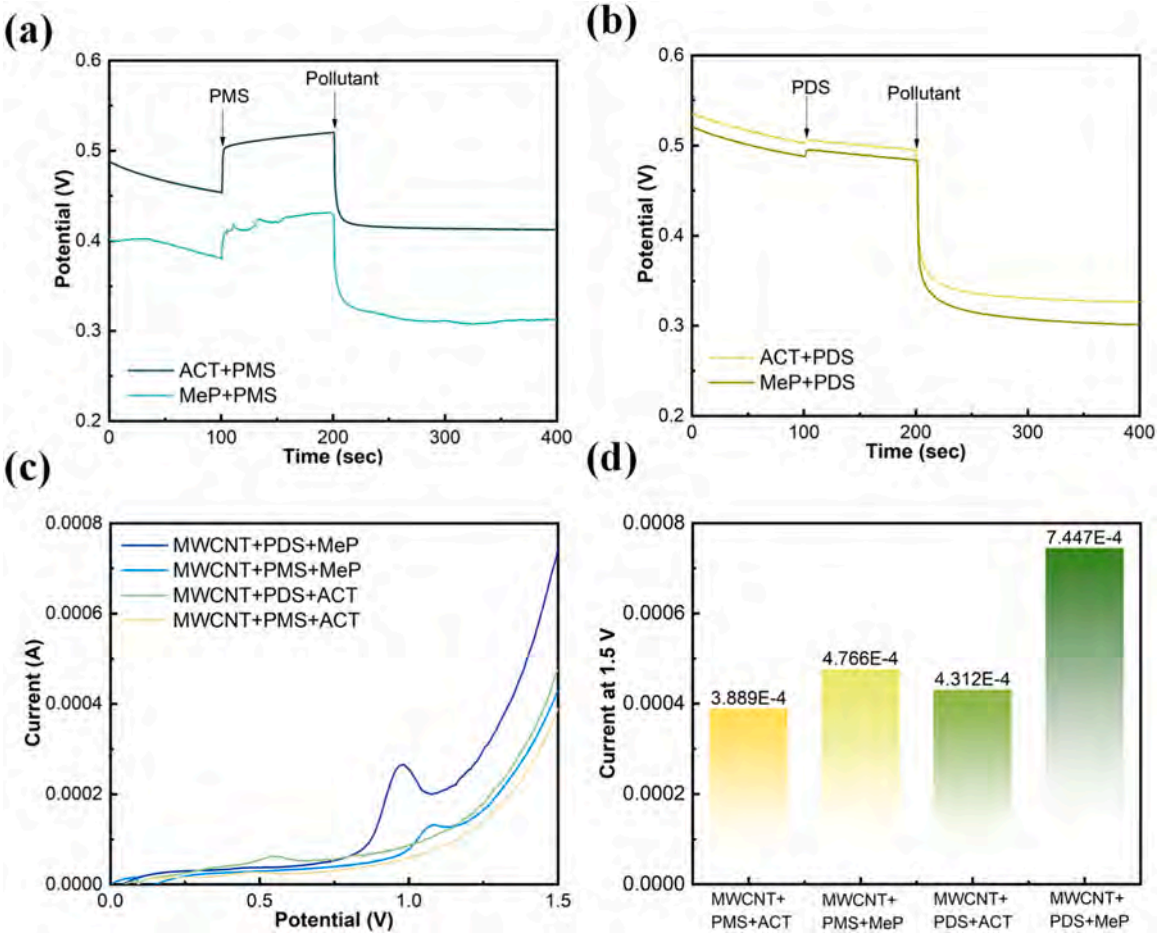

Fig. 3. (a-b) open circuit potential curves on MWCNT decorated electrode at different conditions, (c) LSV measured with the GCE electrode decorated with MWCNT in present of PDS (or PMS) and ACT (or MeP), (d) the responding currents (mA) in LSV analysis at 1.50 V. [Experimental conditions]: [Persulfate]= 4 mM, [Pollutant]= 20 mg/L.

respectively. While in the MWCNT/PDS system, the current reached 4.312×10^{-4} and 7.447×10^{-4} mA, respectively. The PDS-induced degradation process exhibited a higher current compared to the PMS-induced degradation process. It was indicated a stronger electron transfer pathway in the degradation process induced by PDS. When it comes to open circuit potential, the potential decreased by 1.08 V, 1.17 V, 1.69 V, and 1.82 V, in MWCNT/PMS/ACT, MWCNT/PMS/MeP, MWCNT/PDS/ACT, and MWCNT/PDS/MeP, respectively. It also supported a stronger electron transfer pathway in the PDS-induced system. The result was in line with previous studies. Ren and his co-workers reported that the electron transfer pathway degraded organic pollutants by forming a metastable catalyst-persulfate complex, and the complex consisting of PDS obtained a higher oxidation capacity than the complex composed of PMS [58,59]. Moreover, the increase in open circuit potential brought by the introduction of PMS was obviously higher than that of PDS, which corroborated that the contribution of active species in the PMS-induced system was higher than that in the PDS-induced system.

Interestingly, the effect of target pollutants on the variation of LSV and open circuit potential is a pattern. The electrochemical changes of the systems containing MeP was higher than that of the system containing ACT. It was demonstrated that pollutant was another factor affecting the strength of the electron transfer pathway, which might further influence the superior persulfate species [19].

3.3. Correlation between reaction kinetics and properties of phenolic compounds

As mentioned above, in MWCNT/persulfate systems, the effect of the target pollutant on superior persulfate species was observed by ACT and MeP. The difference in degradation mechanisms between MWCNT/PDS and MWCNT/PMS systems ultimately results in the superior persulfate species varied with pollutants. In order to investigate the underlying relationship between the superior persulfate species and the properties of phenolic components, 7 *p*-substituted phenols (MOP, ACT, 4-CP, HAP, MeP, HBAc, and 4-NP) with similar structure and PH were involved. The optimized structure of these 8 phenolic compounds was listed in Fig. S8. The Fukui index was applied to evaluate the reactive sites of phenolic compounds. To be specific, f^+, f^-, and f^0 are associated with nucleophilic, electrophilic, and free-radical attack, respectively, and the high value of f^+, f^-, and f^0 represents a higher likelihood of being attacked [60,61]. Obviously, the f^0 is applied to index the reactive sites on the target pollutant for the radical pathway. Moreover, in the electron transfer pathway, target pollutants act as electron donators, and they are subjected to an electrophilic attack. Thus, the value of f^- is applied to appraise the reactive sites for the electron transfer pathway. As shown in Table S7, 1(C), 4(C) and 7(O) on PH are most vulnerable to be attacked by electrophilic species, and radicals are most likely to attack the carbon atom in the benzene ring. The introduction of para-substituent brought about more reactive sites on target pollutants (Table S5-S12), and the reactive sites for electrophilic attack were widely transferred to the para-substituent. These might finally affect the degradation rate and mechanisms of phenolic compounds in persulfate activation.

To avoid the effects of persulfate self-degradation and adsorption, persulfates and MWCNT were separately introduced in pollutant solution. It could be observed that a single PMS/PDS or MWCNT could not markedly reduce the concentration of these 8 phenolic compounds (Fig. S9). Thus, the decline of pollutant concentration was mainly ascribed to the degradation process in MWCNT/persulfate systems. Apparently, the degradation rates of ACT, MOP, 4-CP, and PH in the MWCNT/PDS system were higher than that of the MWCNT/PMS system (Fig. 4 and Fig. S10). However, the elevation of reactive sites amount did not universally increase the degradation efficiency of target pollutants, and the value of f^+, f^-, and f^0 did not show obvious relation with the superior persulfate species. Thus, the Fukui index could not act as the indication for superior persulfate species in MWCNT/persulfate systems.

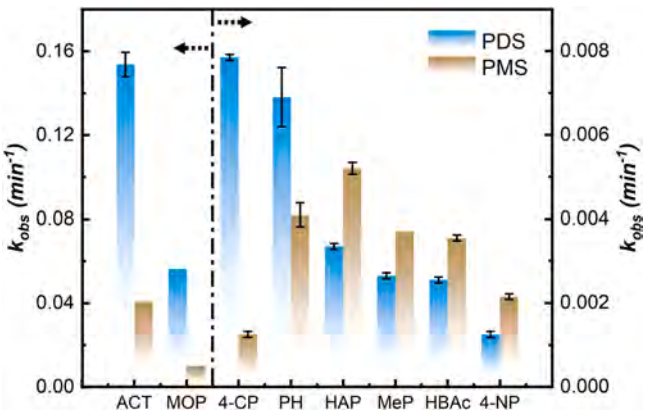

Fig. 4. Catalytic performance with different phenolic compounds of MWCNT/PDS and MWCNT/PMS systems. [Experimental conditions]: [MWCNT]= 0.10 g/L, [Persulfate]= 4 mM, [Pollutant]= 0.20 mM.

Considering target pollutants as a whole, the main distinction of these phenolic compounds was the para-substituents. As is reported, the electron-donating (withdrawing) ability of substituents could influence compound reactivity by changing the electron density [62]. Thus, the electron-donating (withdrawing) ability of substituents might be considered as the factor determining the priority of persulfate species. The electron-withdrawing ability of substituent was -OCH_3 (MOP)< -$NHCOCH_3$ (ACT)< -Cl (4-CP)< -$COCH_3$ (HAP)< -$COOCH_3$ (MeP)< -COOH (HBAc)< -NO_2 (4-NP).

According to the experimental results, when a strong electron-withdrawing substituent was located at the parasite, the degradation capacity of PDS activation systems sharply declined. To dig out a precise conclusion, vertical ionization potential (VIP) and E_{HOMO} (Fig. 5) were involved. Specifically, VIP is associated with the reactivity of the compound and can be applied to quantify the effect of substituent on the compound (electron-withdrawing groups can raise VIP, and electron-donating groups can reduce the VIP) [63]. Moreover, E_{HOMO} can be applied to evaluate the electrophilic reaction activities of compounds [64]. The value of VIP and E_{HOMO} were listed in Table S13. The compounds with electron-withdrawing substituents generally possessed a relatively high VIP and low E_{HOMO}, the electron-donating substituents exhibited the opposite effect. A good linear relationship could be observed between the degradation rate ($\ln k_{obs}$) and the VIP (R^2 =0.9459) (or E_{HOMO} (R^2 =0.9466)) of phenolic components in the MWCNT/PDS system (Fig. 6). Furthermore, the value of VIP (or E_{HOMO}) could also apply as the index for superior persulfate species in MWCNT/persulfate systems. The threshold should emerge at somewhere between PH (VIP=6.397 eV, E_{HOMO}=−7.810 eV) and HAP (VIP=6.674 eV, E_{HOMO}=−8.035 eV). Thus, it could be deduced that VIP= 6.397–6.674 eV (E_{HOMO}=−8.035∼−7.810 eV) were recognized as the threshold of superior persulfate species. That is, when the VIP value was higher than 6.674 eV and the E_{HOMO} value was lower than − 8.035 eV, PMS would be the superior species. Otherwise, when the VIP value was lower than 6.397 eV or the E_{HOMO} value was higher than − 7.810 eV, PDS would be the superior species.

To explore the generalizability of this conclusion, other types of pollutants (BA, NB, and SMX) were introduced. The results of the DFT calculation illustrated that the E_{HOMO} of BA, NB, and SMX was − 8.799, − 9.079, and − 7.659 eV, respectively. The VIP of BA, NB, and SMX was 7.658, 9.256, and 6.503 eV, respectively. Based on the conclusion mentioned above, the superior persulfate species of SMX should be PDS because it possesses above-threshold E_{HOMO} and below-threshold VIP. Accordingly, the superior persulfate species of BA and NB should be PMS. The degradation experiment verified this deduction. As shown in Fig. S4 and Table S13, the SMX degradation efficiency in the MWCNT/PDS system is obviously higher than that of the MWCNT/PMS system.

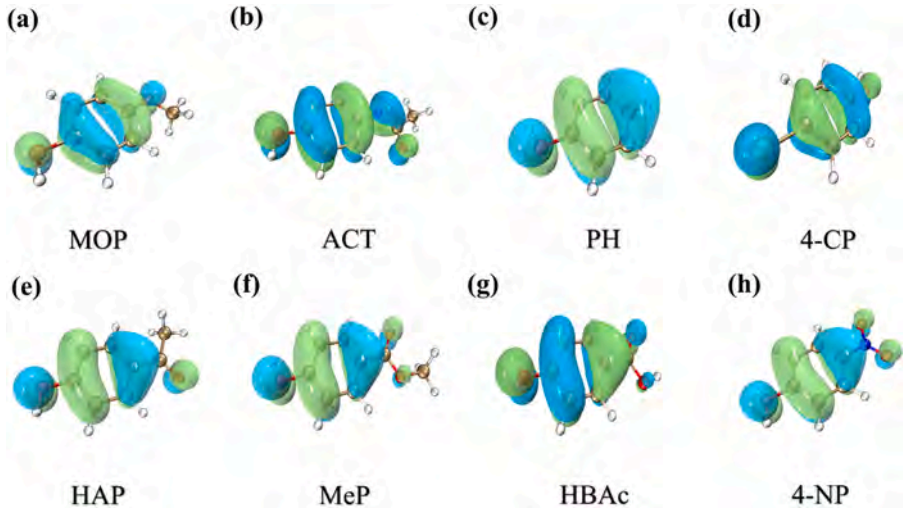

Fig. 5. Spatial charge distributions of HOMO orbit of (a) MOP, (b) ACT, (c) PH, (d) 4-CP, (5) HAP, (6) MeP, (7) HBAc, and (8) 4-NP (isosurface value = 0.02).

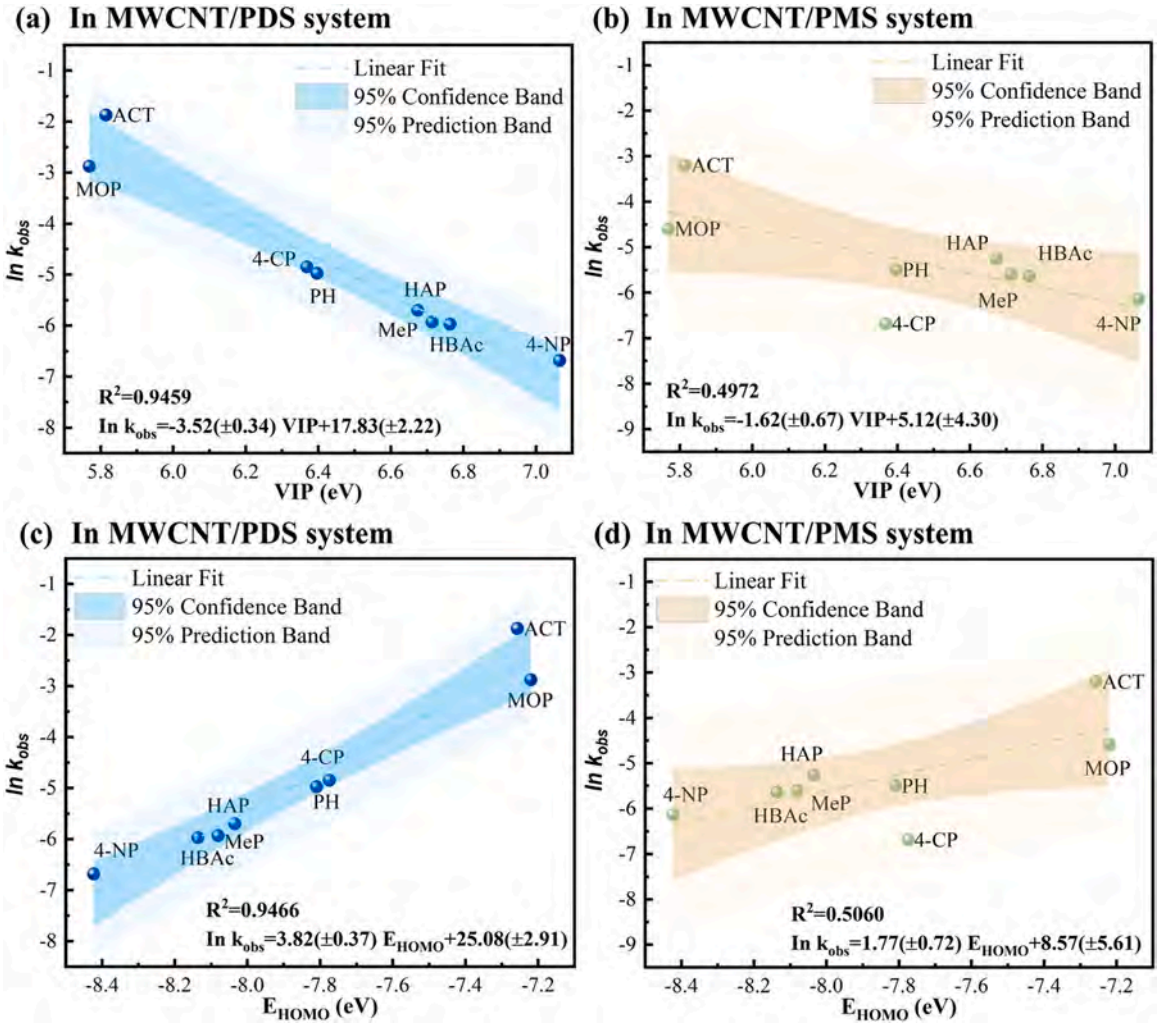

Fig. 6. (a) Correlation of Ink_{obs} and VIP in MWCNT/PDS system, (b) correlation of Ink_{obs} and VIP in MWCNT/PMS system, (c) correlation of Ink_{obs} and E_{HOMO} in MWCNT/PDS system, (d) correlation of Ink_{obs} and E_{HOMO} in MWCNT/PMS system.

The ability of PMS-induced systems to degrade BA and NB is indeed higher than that of PDS-induced systems. It was illustrated that the obtained threshold value is applicable when dealing with other types of target pollutants.

However, the significant correlation between degradation rate and VIP (or E_{HOMO}) has not been embodied in MWCNT/PMS system

(Fig. S12b, S12d). As mentioned above, E_{HOMO} could represent the electrophilic reaction activities of phenolic compounds [65], and the electron transfer process (electrophilic attack) is preferred to take effect in MWCNT/PDS systems rather than in MWCNT/PMS systems. This might be the reason why E_{HOMO} exhibited a better correlation with $\ln k_{obs}$ in MWCNT/PDS system than that in MWCNT/PMS system.

To work out the dominating properties affecting the degradation efficiency in MWCNT/PMS systems, other common indexes were involved. E_{LUMO} (Fig. S11) and ΔE ($\Delta E = E_{LUMO} - E_{HOMO}$) are quantifiable indicators to estimate the reactivity of phenolic compounds. E_{LUMO} indicates the nucleophilic reaction ability and ΔE is associated with kinetic stability [65,66]. However, the linear fitting results illustrated that the nucleophilic reaction ability and kinetic stability did not play a role in either MWCNT/PDS or MWCNT/PMS system (Fig. S12).

Aside from the physicochemical characteristics obtained from DFT theoretical calculation, hydrophobicity was another property that would influence the degradation rate of phenolic components in the persulfate activation system. Mao and co-workers proved that the pollutant with high hydrophobicity would occupy the more active site on the catalyst, which ultimately resulted in a higher degradation rate [21]. In order to achieve the quantification, Wang et al. developed a method based on atom (Xlog P) to predict the hydrophobicity of organic compounds (The detail of Xlog P is presented in Section 2.3) [67]. As shown in Fig. S12f, $\ln k_{obs}$ exhibited a good linear relationship with Xlog P in MWCNT/PMS system (R^2 =0.9189). Different from the positive correlation reported in the previous study, $\ln k_{obs}$ decreased with the lift of the Xlog P value in this study. It might account for the difference in degradation mechanism induced by different persulfates. Compared to MWCNT/PDS systems, active species played a greater role in the MWCNT/PMS system. The contact between target pollutants and free active species in water is closely related to the hydrophobicity of organic compounds. Thus, the degradation efficiency presented a good correlation with the hydrophobicity of organic compounds in the MWCNT/PMS system. However, apparently, different from VIP (or E_{HOMO}), the Xlog P could hardly be denoted as the indicator for superior persulfate species.

To sum up, the electron transfer process dominated the MWCNT/PDS system, thus the VIP (or E_{HOMO}) correlated well with $\ln k_{obs}$. Similarly, the Xlog P value had a good correlation with $\ln k_{obs}$ for the radical pathway that played a greater role in MWCNT/PMS system. However, among the mentioned characteristics, only the value of VIP (or E_{HOMO}) decided the superior persulfate species in MWCNT/persulfate systems, and the threshold was VIP= 6.397–6.674 and E_{HOMO}= −8.035∼− 7.810 (Fig. 7).

3.4. The superior peroxydisulfate species

Aside from potassium persulfates (PDS and PMS), PDS-Na and PDS-NH_4, are also universally applied as oxidants in the persulfate activation system [68,69]. Although the PDSs (PDS, PDS-Na, and PDS-NH_4) share the same main effective component ($S_2O_8^{2-}$), the different coexisting cations may make some changes. Identifying the effects of coexisting cations on the degradation efficiency of the persulfate activation system is also of great significance.

Similarly, the thermal activation system was applied to investigate the effect of oxidant properties on superior persulfate species. An evident difference in degradation efficiency can be seen in the thermal activation system (Table S3 and Fig. S13). For both ACT and MeP, the order of degradation performance order was the same: PDS-Na>PDS>PDS-NH_4. This phenomenon manifested that the co-existing cation affected the pollutant degradation rate, and this effect was independent of the pollutant. It has been reported that the hydrated cation radius of monovalent cations could influence the relative electrostatic shielding of compounds, which might finally act on thermal stability. A larger hydrated cation radius might lead to lower thermal stability [70,71]. As for the monovalent cations in common PDSs, the hydrated cation radius of Na^+, K^+, and NH_4^+ was 0.358 nm, 0.331 nm, and 0.330 nm, respectively [72]. This implied that the thermal stability of PDSs was ranked as PDS-Na<PDS<PDS-NH_4, which was consistent with the degradation performance order of the thermal activation system.

However, when MWCNT was involved, the influence of cation size on degradation rate could not be observed (Fig. 8 and Fig. S14). This might be because the degradation process in MWCNT/PDSs systems was dominated by the electron transfer pathway, which relied on the contact of MWCNT with PDSs and pollutants. Thus, the difference in PDSs thermal stability caused by coexisting cations is weakened.

4. Conclusions

Although the O-O bond in PDS is more fragile than that of PMS, and the degradation efficiency of the PDS-induced system is not consistently superior to that of the PMS activation system. This study investigated the effect of target phenolic compounds on superior persulfate species. On account of the difference in degradation mechanism proportion, the degradation rate of different phenolic compounds in PDS and PMS activation systems presented different trends. In MWCNT/persulfate systems, while VIP (or E_{HOMO}) of target pollutants dominated the degradation efficiency of MWCNT/PDS systems, hydrophobicity was the

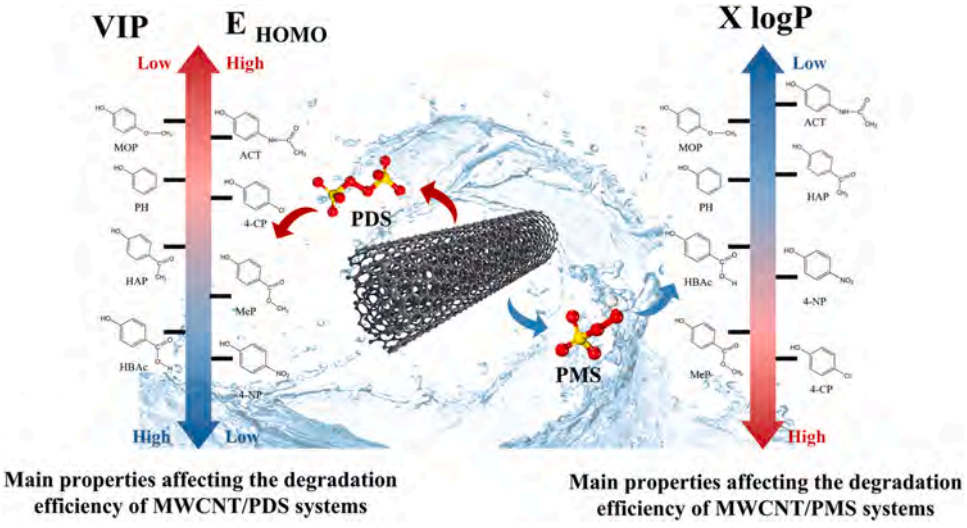

Fig. 7. The main pollutant properties affecting the degradation efficiency of MWCNT/PDS and MWCNT/PMS systems, and the ranking of relevant properties of the introduced pollutants.

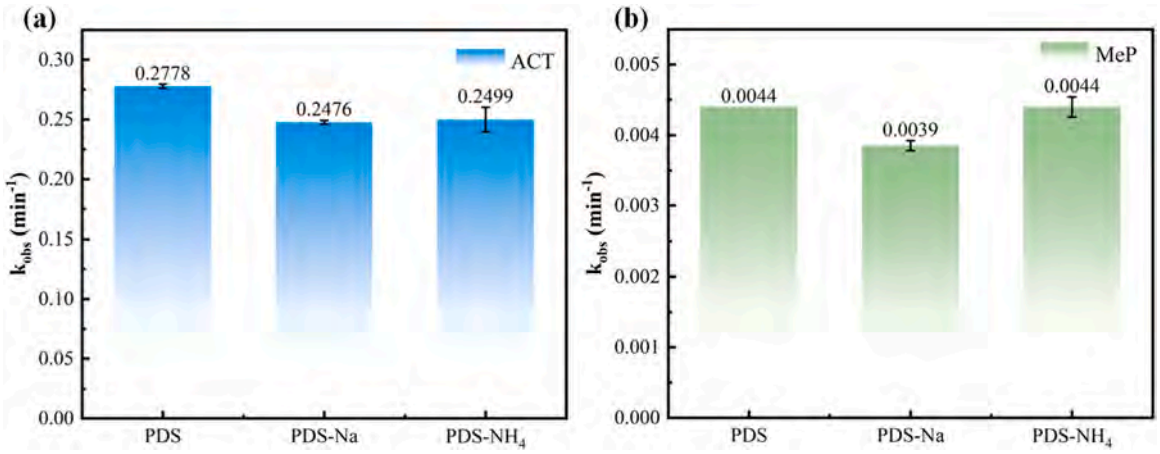

Fig. 8. (a) ACT degradation rate in MWCNT/PDSs systems, (b) MeP degradation rate in MWCNT/PDSs systems [Experimental conditions]: [MWCNT]= 0.1 g/L, [Persulfate]= 4 mM, [Pollutant]= 20 mg/L.

main properties influence the degradation efficiency in MWCNT/PMS systems. Moreover, the value of VIP (or E_{HOMO}) could be regarded as the threshold of superior persulfate species. Specifically, the threshold was VIP= 6.397–6.674 and E_{HOMO}= −8.035~− 7.810. This result is only valid in MWCNT/persulfate systems. To emphasize the vision of green development, it is necessary to investigate the superior persulfate species in different reaction systems. Furthermore, in a homogeneous catalytic (thermal activation) system, the size of co-existing cations size would influence the thermal stability of PDS, which would ultimately act on the degradation efficiency. However, this effect was not embodied in a heterogeneous catalytic (MWCNT/persulfate) system. Thus, the option of PDSs in heterogeneous catalytic systems could ignore the influence of co-existing cations on degradation efficiency to some extent. Overall, the option of persulfate is another emerging key point for the green development of AOPs, it is necessary to focus on the superior persulfate species for different persulfate activation systems.

Environmental Implications

At present, the research on improving the cost-efficiency of persulfate activation system mainly focuses on the modification of catalysts, the option of persulfates is rarely reported. In this study, the multiwalled carbon nanotube (MWCNT)/persulfate system was denoted as the model system to investigate the effect of pollutants on superior persulfate species. It was illustrated that EHOMO, vertical ionization potential (VIP), and hydrophobicity were closely related to the degradation efficiency under certain conditions. Moreover, EHOMO and VIP could be recognized as the index for superior persulfate species. This verdict provides a new perspective for the design of efficient persulfate activation technology.

CRediT authorship contribution statement

Xuerong Zhou: Writing, Methodology, Conceptualization, Formal analysis, Writing – original draft. **Eydhah Almatrafi:** Methodology, Writing – review & editing. **Shiyu Liu:** Methodology, Writing – review & editing. **Huchuan Yan:** Investigation, Writing – review & editing. **Dengsheng Ma:** Methodology, Writing – review & editing. **Shixian Qian:** Investigation, Writing – review & editing. **Lei Qin:** Investigation, Writing – review & editing. **Huan Yi:** Investigation, Writing – review & editing. **Yukui Fu:** Methodology, Writing – review & editing. **Ling Li:** Methodology, Writing – review & editing. **Mingming Zhang:** Methodology, Writing – review & editing. **Fuhang Xu:** Methodology, Investigation, Formal analysis. **Hanxi Li:** Investigation, Writing – review & editing. **Chengyun Zhou:** Investigation, Writing – review & editing. **Ming Yan:** Methodology, Investigation, Formal analysis. **Cui Lai:** Writing, Methodology, Investigation, Writing – review & editing. **Guangming Zeng:** Writing, Methodology, Investigation, Writing – review & editing.

Declaration of Competing Interest

The authors declare that they have no known competing financial interests or personal relationships that could have appeared to influence the work reported in this paper.

Data Availability

Data will be made available on request.

Acknowledgements

This study was financially supported by the Program for the National Natural Science Foundation of China (U20A20323, 52170161, 52100182, 52100183), the National Program for Support of Top–Notch Young Professionals of China (2014), the Program for Changjiang Scholars and Innovative Research Team in University (IRT-13R17). The Program for Ecological restoration and engineering in Chinese Academy of Sciences, Chongqing (E055620201), the Hunan Natural Science Foundation (2022JJ40044), the Hunan Researcher Award Program (2020RC3025), the Project funded by China Postdoctoral Science Foundation (2021M700041), Postgraduate Scientific Research Innovation Project of Hunan Province (CX20230447), and Changsha Municipal Natural Science Foundation (kq2202166).

Appendix A. Supporting information

Supplementary data associated with this article can be found in the online version at doi:10.1016/j.jhazmat.2023.132363.

References

[1] Masud, M.A.A., Narendra Kumar, A.V., Shin, W.S., 2023. Fe(II) activated calcium peroxide/peroxymonosulfate: a practical system for phenanthrene degradation and upholding ecological pH. Sep Purif Technol 317, 123902.
[2] Li, L., Liu, S., Cheng, M., Lai, C., Zeng, G., Qin, L., et al., 2021. Improving the Fenton-like catalytic performance of MnOx-Fe3O4/biochar using reducing agents: a comparative study. J Hazard Mater 406, 124333.
[3] Fu, Y., Yin, Z., Qin, L., Huang, D., Yi, H., Liu, X., et al., 2022. Recent progress of noble metals with tailored features in catalytic oxidation for organic pollutants degradation. J Hazard Mater 422, 126950.
[4] Yi, H., Lai, C., Huo, X., Qin, L., Fu, Y., Liu, S., et al., 2022. H2O2-free photo-Fenton system for antibiotics degradation in water via the synergism of oxygen-enriched graphitic carbon nitride polymer and nano manganese ferrite. Environ Sci: Nano 9, 815–826.

[5] Wang, D., He, N., Xiao, L., Dong, F., Chen, W., Zhou, Y., et al., 2021. Coupling electrocatalytic nitric oxide oxidation over carbon cloth with hydrogen evolution reaction for nitrate synthesis. Angew Chem 133, 24810–24816.

[6] Zhang, M., Lai, C., Li, B., Xu, F., Huang, D., Liu, S., et al., 2020. Unravelling the role of dual quantum dots cocatalyst in 0D/2D heterojunction photocatalyst for promoting photocatalytic organic pollutant degradation. Chem Eng J 396, 125343.

[7] Xu, F., Lai, C., Zhang, M., Li, B., Liu, S., Chen, M., et al., 2021. Facile one-pot synthesis of carbon self-doped graphitic carbon nitride loaded with ultra-low ceric dioxide for high-efficiency environmental photocatalysis: Organic pollutants degradation and hexavalent chromium reduction. J Colloid Interface Sci 601, 196–208.

[8] Lai, C., An, Z., Yi, H., Huo, X., Qin, L., Liu, X., et al., 2021. Enhanced visible-light-driven photocatalytic activity of bismuth oxide via the decoration of titanium carbide quantum dots. J Colloid Interface Sci 600, 161–173.

[9] Zhang, M.M., Lai, C., Li, B.S., Xu, F.H., Huang, D.L., Liu, S.Y., et al., 2021. Insightful understanding of charge carrier transfer in 2D/2D heterojunction photocatalyst: Ni-Co layered double hydroxides deposited on ornamental g-C3N4 ultrathin nanosheet with boosted molecular oxygen activation. Chem Eng J 422.

[10] von Gunten, U., 2003. Ozonation of drinking water: Part I. Oxidation kinetics and product formation. Water Res 37, 1443–1467.

[11] Ma, D., Yi, H., Lai, C., Liu, X., Huo, X., An, Z., et al., 2021. Critical review of advanced oxidation processes in organic wastewater treatment. Chemosphere 275, 130104.

[12] Lai, C., Yan, H., Wang, D., Liu, S., Zhou, X., Li, X., et al., 2022. Facile synthesis of Mn, Ce co-doped g-C3N4 composite for peroxymonosulfate activation towards organic contaminant degradation. Chemosphere 293, 133472.

[13] Liu, S., Lai, C., Zhou, X., Zhang, C., Chen, L., Yan, H., et al., 2022. Peroxydisulfate activation by sulfur-doped ordered mesoporous carbon: Insight into the intrinsic relationship between defects and (1)O2 generation. Water Res 221, 118797.

[14] Miao, J., Geng, W., Alvarez, P.J., Long, M., 2020. 2D N-doped porous carbon derived from polydopamine-coated graphitic carbon nitride for efficient nonradical activation of peroxymonosulfate. Environ Sci Technol 54, 8473–8481.

[15] Zhou, X., Zhu, Y., Niu, Q., Zeng, G., Lai, C., Liu, S., et al., 2021. New notion of biochar: a review on the mechanism of biochar applications in advannced oxidation processes. Chem Eng J 416.

[16] Duan, X., Ao, Z., Sun, H., Zhou, L., Wang, G., Wang, S., 2015. Insights into N-doping in single-walled carbon nanotubes for enhanced activation of superoxides: a mechanistic study. Chem Commun 51, 15249–15252.

[17] Zhou, X., Lai, C., Liu, S., Li, B., Qin, L., Liu, X., et al., 2022. Activation of persulfate by swine bone derived biochar: Insight into the specific role of different active sites and the toxicity of acetaminophen degradation pathways. Sci Total Environ 807, 151059.

[18] Guan, C., Jiang, J., Luo, C., Pang, S., Yang, Y., Wang, Z., et al., 2018. Oxidation of bromophenols by carbon nanotube activated peroxymonosulfate (PMS) and formation of brominated products: comparison to peroxydisulfate (PDS). Chem Eng J 337, 40–50.

[19] Ren, W., Xiong, L., Yuan, X., Yu, Z., Zhang, H., Duan, X., et al., 2019. Activation of peroxydisulfate on carbon nanotubes: electron-transfer mechanism. Environ Sci Technol 53, 14595–14603.

[20] Xie, Z.H., He, C.S., Zhou, H.Y., Li, L.L., Liu, Y., Du, Y., et al., 2022. Effects of molecular structure on organic contaminants' degradation efficiency and dominant ROS in the advanced oxidation process with multiple ROS. Environ Sci Technol 56, 8784–8795.

[21] Liu, X., Liu, Y., Qin, H., Ye, Z., Wei, X., Miao, W., et al., 2022. Selective removal of phenolic compounds by peroxydisulfate activation: inherent role of hydrophobicity and interface ROS. Environ Sci Technol 56, 2665–2676.

[22] Zhang, L.-C., Jia, Z., Lyu, F., Liang, S.-X., Lu, J., 2019. A review of catalytic performance of metallic glasses in wastewater treatment: Recent progress and prospects. Prog Mater Sci 105, 100576.

[23] Nain, P., Kumar, A., 2020. Ecological and human health risk assessment of metals leached from end-of-life solar photovoltaics. Environ Pollut 267, 115393.

[24] Zhou, X., Zeng, Z., Zeng, G., Lai, C., Xiao, R., Liu, S., et al., 2020. Insight into the mechanism of persulfate activated by bone char: unraveling the role of functional structure of biochar. Chem Eng J 401, 126127.

[25] Liu, S., Lai, C., Liu, X., Li, B., Zhang, C., Qin, L., et al., 2020. Metal-organic frameworks and their derivatives as signal amplification elements for electrochemical sensing. Coord Chem Rev 424.

[26] Lee, H., Lee, H.-J., Jeong, J., Lee, J., Park, N.-B., Lee, C., 2015. Activation of persulfates by carbon nanotubes: Oxidation of organic compounds by nonradical mechanism. Chem Eng J 266, 28–33.

[27] Duan, X., Sun, H., Kang, J., Wang, Y., Indrawirawan, S., Wang, S., 2015. Insights into heterogeneous catalysis of persulfate activation on dimensional-structured nanocarbons. ACS Catal 5, 4629–4636.

[28] Li, Y., Fu, Y., Lai, C., Qin, L., Li, B., Liu, S., et al., 2021. Porous materials confining noble metals for the catalytic reduction of nitroaromatics: controllable synthesis and enhanced mechanism. Environ Sci-Nano 8, 3067–3097.

[29] Masud, M.A.A., Shin, W.S., Kim, D.G., 2023. Degradation of phenol by ball-milled activated carbon (ACBM) activated dual oxidant (persulfate/calcium peroxide) system: effect of preadsorption and sequential injection. Chemosphere 312, 137120.

[30] Masud, M.A.A., Kim, D.G., Shin, W.S., 2022. Degradation of phenol using Fe(II)-activated CaO2: effect of ball-milled activated carbon (ACBM) addition. Environ Res 214, 113882.

[31] Masud, M.A.A., Kim, D.G., Shin, W.S., 2022. Highly efficient degradation of phenolic compounds by Fe(II)-activated dual oxidant (persulfate/calcium peroxide) system. Chemosphere 299, 134392.

[32] Masud, M.A.A., Annamalai, S., Shin, W.S., 2023. Remediation of ciprofloxacin in soil using peroxymonosulfate activated by ball-milled seaweed kelp biochar: Performance, mechanism, and phytotoxicity. Chem Eng J 465, 142908.

[33] Masud, M.A.A., Shin, W.S., Kim, D.G., 2023. Fe-doped kelp biochar-assisted peroxymonosulfate activation for ciprofloxacin degradation: Multiple active site-triggered radical and non-radical mechanisms. Chem Eng J 471, 144519.

[34] Me Frisch , G. Trucks , H. Schlegel , G. Scuseria , M. Robb , J. Cheeseman , , , , et al. , Gaussian 16, in, Gaussian, Inc. Wallingford, CT, 2016.

[35] Lee, C., Yang, W., Parr, R.G., 1988. Development of the Colle-Salvetti correlation-energy formula into a functional of the electron density. PhRvB 37, 785–789.

[36] Grimme, S., Antony, J., Ehrlich, S., Krieg, H., 2010. A consistent and accurate ab initio parametrization of density functional dispersion correction (DFT-D) for the 94 elements H-Pu. J Chem Phys 132.

[37] Becke, A.D., 1988. Density-functional exchange-energy approximation with correct asymptotic behavior. Phys Rev A 38, 3098–3100.

[38] Zhao, Y., Truhlar, D.G., 2008. The M06 suite of density functionals for main group thermochemistry, thermochemical kinetics, noncovalent interactions, excited states, and transition elements: two new functionals and systematic testing of four M06-class functionals and 12 other functionals. Theor Chem Acc 120, 215–241.

[39] Tomasi, J., Mennucci, B., Cammi, R., 2005. Quantum mechanical continuum solvation models. Chem Rev 105, 2999–3094.

[40] Humphrey, W., Dalke, A., Schulten, K., 1996. VMD: visual molecular dynamics. J Mol Graph 14, 33–38.

[41] Lu, T., Chen, F., 2012. Multiwfn: a multifunctional wavefunction analyzer. J Comput Chem 33, 580–592.

[42] Antunes, E.F., Lobo, A.O., Corat, E.J., Trava-Airoldi, V.J., Martin, A.A., Veríssimo, C., 2006. Comparative study of first- and second-order Raman spectra of MWCNT at visible and infrared laser excitation. Carbon 44, 2202–2211.

[43] Kuznetsov, V.L., Bokova-Sirosh, S.N., Moseenkov, S.I., Ishchenko, A.V., Krasnikov, D.V., Kazakova, M.A., et al., 2014. Raman spectra for characterization of defective CVD multi-walled carbon nanotubes. Phys Status Solidi (b) 251, 2444–2450.

[44] Okpalugo, T.I.T., Papakonstantinou, P., Murphy, H., McLaughlin, J., Brown, N.M. D., 2005. High resolution XPS characterization of chemical functionalised MWCNTs and SWCNTs. Carbon 43, 153–161.

[45] Gardella, J.A., Ferguson, S.A., Chin, R.L., 1986. $\pi^* \leftarrow \pi$ shakeup satellites for the analysis of structure and bonding in aromatic polymers by X-ray photoelectron spectroscopy. Appl Spectrosc 40, 224–232.

[46] Asano, M., Iwahashi, H., 2014. Caffeic acid inhibits the formation of 7-carboxy-heptyl radicals from oleic acid under flavin mononucleotide photosensitization by scavenging singlet oxygen and quenching the excited state of flavin mononucleotide. Molecules 19, 12486–12499.

[47] Hu, P., Su, H., Chen, Z., Yu, C., Li, Q., Zhou, B., et al., 2017. Selective degradation of organic pollutants using an efficient metal-free catalyst derived from carbonized polypyrrole via peroxymonosulfate activation. Environ Sci Technol 51, 11288–11296.

[48] Zhang, Y., Fan, J., Yang, B., Huang, W., Ma, L., 2017. Copper-catalyzed activation of molecular oxygen for oxidative destruction of acetaminophen: the mechanism and superoxide-mediated cycling of copper species. Chemosphere 166, 89–95.

[49] Nosaka, Y., Nosaka, A.Y., 2017. Generation and detection of reactive oxygen species in photocatalysis. Chem Rev 117, 11302–11336.

[50] Tratnyek, P.G., Hoigne, J., 1991. Oxidation of substituted phenols in the environment: a QSAR analysis of rate constants for reaction with singlet oxygen. Environ Sci Technol 25, 1596–1604.

[51] Yun, E.-T., Lee, J.H., Kim, J., Park, H.-D., Lee, J., 2018. Identifying the nonradical mechanism in the peroxymonosulfate activation process: singlet oxygenation versus mediated electron transfer. Environ Sci Technol 52, 7032–7042.

[52] Oh, W.-D., Dong, Z., Lim, T.-T., 2016. Generation of sulfate radical through heterogeneous catalysis for organic contaminants removal: current development, challenges and prospects. Appl Catal B: Environ 194, 169–201.

[53] Zhang, M., Lai, C., Li, B., Xu, F., Huang, D., Liu, S., et al., 2020. Unravelling the role of dual quantum dots cocatalyst in 0D/2D heterojunction photocatalyst for promoting photocatalytic organic pollutant degradation. Chem Eng J 396, 125343.

[54] Chen, Y., Deng, P., Xie, P., Shang, R., Wang, Z., Wang, S., 2017. Heat-activated persulfate oxidation of methyl- and ethyl-parabens: Effect, kinetics, and mechanism. Chemosphere 168, 1628–1636.

[55] Liu, S., Lai, C., Li, B., Zhang, C., Zhang, M., Huang, D., et al., 2020. Role of radical and non-radical pathway in activating persulfate for degradation of p-nitrophenol by sulfur-doped ordered mesoporous carbon. Chem Eng J 384.

[56] Ren, W., Zhang, Q., Cheng, C., Miao, F., Zhang, H., Luo, X., et al., 2022. Electro-induced carbon nanotube discrete electrodes for sustainable persulfate activation. Environ Sci Technol 56, 14019–14029.

[57] Cheng, X., Guo, H., Zhang, Y., Korshin, G.V., Yang, B., 2019. Insights into the mechanism of nonradical reactions of persulfate activated by carbon nanotubes: activation performance and structure-function relationship. Water Res 157, 406–414.

[58] Ren, W., Nie, G., Zhou, P., Zhang, H., Duan, X., Wang, S., 2020. The intrinsic nature of persulfate activation and N-doping in carbocatalysis. Environ Sci Technol 54, 6438–6447.

[59] Ren, W., Xiong, L., Nie, G., Zhang, H., Duan, X., Wang, S., 2020. Insights into the electron-transfer regime of peroxydisulfate activation on carbon nanotubes: the role of oxygen functional groups. Environ Sci Technol 54, 1267–1275.

[60] Oláh, J., Van Alsenoy, C., Sannigrahi, A.B., 2002. Condensed fukui functions derived from stockholder charges: assessment of their performance as local reactivity descriptors. J Phys Chem A 106, 3885–3890.

[61] Peng, J., Zhou, H., Liu, W., Ao, Z., Ji, H., Liu, Y., et al., 2020. Insights into heterogeneous catalytic activation of peroxymonosulfate by natural chalcopyrite: pH-dependent radical generation, degradation pathway and mechanism. Chem Eng J 397, 125387.
[62] Lee, C.Y., Anamoah, C., Semenya, J., Chapman, K.N., Knoll, A.N., Brinkman, H.F., et al., 2020. Electronic (donating or withdrawing) effects of ortho-phenolic substituents in dendritic antioxidants. Tetrahedron Lett 61, 151607.
[63] Wright, J.S., Johnson, E.R., DiLabio, G.A., 2001. Predicting the activity of phenolic antioxidants: theoretical method, analysis of substituent effects, and application to major families of antioxidants. J Am Chem Soc 123, 1173–1183.
[64] Wang, N., Zhu, L., Huang, Y., She, Y., Yu, Y., Tang, H., 2009. Drastically enhanced visible-light photocatalytic degradation of colorless aromatic pollutants over TiO2 via a charge-transfer-complex path: a correlation between chemical structure and degradation rate of the pollutants. J Catal 266, 199–206.
[65] Aihara, J.-i, 1999. Weighted HOMO-LUMO energy separation as an index of kinetic stability for fullerenes. Theor Chem Acc 102, 134–138.
[66] Yin, R., Guo, W., Ren, N., Zeng, L., Zhu, M., 2020. New insight into the substituents affecting the peroxydisulfate nonradical oxidation of sulfonamides in water. Water Res 171, 115374.
[67] Wang, R., Fu, Y., Lai, L., 1997. A new atom-additive method for calculating partition coefficients. J Chem Inf Comput Sci 37, 615–621.
[68] Bekris, L., Frontistis, Z., Trakakis, G., Sygellou, L., Galiotis, C., Mantzavinos, D., 2017. Graphene: a new activator of sodium persulfate for the advanced oxidation of parabens in water. Water Res 126, 111–121.
[69] Li, X., Yu, Z., Chen, Q., Wang, C., Ma, L., Shen, G., 2022. Kill three birds with one stone: iron-doped graphitic biochar from biogas residues for ammonium persulfate activation to simultaneously degrade benzo [a] pyrene and improve lettuce growth. Chem Eng J 430, 132844.
[70] Stellwagen, E., Muse, J.M., Stellwagen, N.C., 2011. Monovalent cation size and DNA conformational stability. Biochemistry 50, 3084–3094.
[71] Skogareva, L.S., Minaeva, N.A., Filippova, T.V., 2009. Synthesis, vibrational spectra, and structure of divalent metal peroxodisulfates. Russ J Inorg Chem 54, 1341–1349.
[72] Nightingale Jr, E., 1959. Phenomenological theory of ion solvation. Effective radii of hydrated ions. J Phys Chem 63, 1381–1387.